Chemistry–A European Journal
Research Article
doi.org/10.1002/chem.202303254
Chemistry Europe
European Chemical Societies Publishing
www.chemeurj.org

In vitro Production of Hemin-Based Artificial Metalloenzymes

Rocío López-Domene[+],[a, b] Aitor Manteca[+],[a] Andoni Rodriguez-Abetxuko,[b] Ana Beloqui,*[b, c] and Aitziber L. Cortajarena*[a, c]

This article is part of the Special Collection in Chemistry – A European Journal and the European Journal of Organic Chemistry to honor Professor Maurizio Prato

Developing enzyme alternatives is pivotal to improving and enabling new processes in biotechnology and industry. Artificial metalloenzymes (ArMs) are combinations of protein scaffolds with metal elements, such as metal nanoclusters or metal-containing molecules with specific catalytic properties, which can be customized. Here, we engineered an ArM based on the consensus tetratricopeptide repeat (CTPR) scaffold by introducing a unique histidine residue to coordinate the hemin cofactor. Our results show that this engineered system exhibits robust peroxidase-like catalytic activity driven by the hemin. The expression of the scaffold and subsequent coordination of hemin was achieved by recombinant expression in bulk and through in vitro transcription and translation systems in water-in-oil drops. The ability to synthesize this system *in emulsio* paves the way to improve its properties by means of droplet microfluidic screenings, facilitating the exploration of the protein combinatorial space to discover improved or novel catalytic activities.

Introduction

Artificial metalloenzymes (ArMs) are hybrid biomacromolecules that combine the selectivity properties of natural enzymes with the tunability of transition metal catalysts.[1] ArMs consist of a proteogenic scaffold combined with a metal cofactor, which serves as artificial catalytic site, and have demonstrated the ability to catalyze a wide range of reactions.[2] Examples include carbonic anhydrases[3] (using a zinc ion cofactor), superoxide dismutases[4] (copper and zinc), nitrogenases[5] (iron and molybdenum), and the water splitting enzyme Photosystem II[6] (manganese). Overall, ArMs have the potential to revolutionize catalysis in many fields, including industrial, medical, and biotechnological applications.

In this context, finding versatile protein scaffolds is crucial for designing ArMs. Repeat proteins can combine tandem repeats of a specific amino acid sequence with known structures. For instance, one such example is the tetratricopeptide repeat (TPR) protein, which is found in many eukaryotic organisms and takes part in several protein-protein interactions.[7] The consensus version of TPR (CTPR) allows the insertion of multiple tandem repeats and permits the mutation of numerous residues within the same repeat without compromising its structure.[8] Consequently, it becomes possible to introduce an amino acid at a precise position that can eventually serve as a metal-binding site within the protein scaffold. Due to the high mutability of these proteins, the binding pocket can also be finely tuned to better allocate a metal-containing molecule.

Heme peroxidases are a subclass of iron-based peroxidases that contain a heme prosthetic group in their catalytic site. This heme molecule, composed of an iron porphyrin complex, is responsible for binding and activating hydrogen peroxide (H_2O_2),[9] for the subsequent oxidation of small organic substrates.[10] Some examples of this kind of enzyme are the catalases, the myeloperoxidases, and the extensively used horseradish peroxidase[11] (HRP). The primary function of these enzymes is to reduce peroxides into water and oxygen, being pivotal in removing harmful peroxides from cells and tissues. They also contribute to the biosynthesis of hormones,[12] cellular signalling,[13] and defense against certain pathogens.[14]

Inspired by nature and driven by the need to create artificial catalysts, which can overcome certain limitations of natural

[a] R. López-Domene,[+] Dr. A. Manteca,[+] Prof. A. L. Cortajarena
Centre for Cooperative Research in Biomaterials (CIC biomaGUNE)
Basque Research and Technology Alliance (BRTA)
Paseo de Miramón 194, Donostia-San Sebastián, E-20014 Spain
E-mail: alcortajarena@cicbiomagune.es
Homepage: http://personal.cicbiomagune.es/alcortajarena/

[b] R. López-Domene,[+] Dr. A. Rodriguez-Abetxuko, Dr. A. Beloqui
POLYMAT and Department of Applied Chemistry, Faculty of Chemistry
University of the Basque Country UPV/EHU,
Donostia-San Sebastián, E-20018 Spain
E-mail: ana.beloquie@ehu.eus
Homepage: https://anabeloqui1982.wixsite.com/polyzymes

[c] Dr. A. Beloqui, Prof. A. L. Cortajarena
IKERBASQUE, Basque Foundation for Science
Plaza Euskadi 5, E-48009 Bilbao, Spain

[+] These authors contributed equally to this work.

Supporting information for this article is available on the WWW under https://doi.org/10.1002/chem.202303254

catalysts – including stability and performance under broad operational conditions –, previous studies have focused on engineering supramolecular scaffolds based on heme-type catalysts. These scaffolds include molecular building blocks of DNA,[15] polymers,[16–18] or proteins. Regarding the proteogenic scaffolds, attempts to generate an artificial heme-protein include enzyme repurposing strategies with specific metal salts,[19] short peptides to coordinate heme groups,[20,21] or the engineering of a *de novo* four-helix bundle protein to coordinate diiron molecules.[22] These studies have demonstrated the potential of integrating metal catalysts within biomolecular scaffolds to create novel catalytic systems.

In this sense, the catalytic potential of CTPR proteins has yet to be explored. In a previously reported work, CTPR proteins were utilized for catalytic applications, enabling the catalysis of reactions beyond the scope of natural enzymes. Specifically, the designed protein acted as metal-free biocatalysts for (3 + 2) cycloadditions.[23] Our group also demonstrated the capability of CTPR proteins to act as scaffolds for coordinating metal nanoclusters, achieving tunable, highly catalytic, stable, and reusable nanozymes, proving them as an advantageous alternative to natural enzymes.[24] This study presents a new approach: the development of an engineered CTPR3 variant with the capacity to coordinate a hemin porphyrin, simulating the structural conformation of HRP. This novel approach emphasizes our endeavours to harness engineered CTPR proteins in multifaceted catalytic contexts.

However, there are still open challenges to overcome and ensure the efficient and broad applicability of this concept, including: 1) ensuring the stability of the ArM upon engineering; 2) assessing the versatility of the protein scaffold to accommodate assorted metal-porphyrins; 3) facilitating efficient substrate accessibility for optimal catalytic activity; and 4) implementing high-throughput techniques to transition from individual ArM design and analysis to the combinatorial generation and screening of ArMs. Towards these aims, in this work, we employed a highly stable CTPR module with three repeats and an engineered histidine site ($CTPR3_H$) to coordinate metal porphyrin complexes, including iron porphyrin compound – hemin – with peroxidative potential. The selection of this scaffold was based on its remarkable stability, engineerability, and superhelical structure, which presents an inner concave face,[27] offering potential for coordination and stabilization of cofactors. The proposed design leads to the generation of an artificial biocatalyst which catalytic pocket is accessible to the solvent (Figure 1A). Our results reveal $CTPR3_H$ as an excellent and versatile platform for engineering ArMs based on metal-porphyrins. Furthermore, we successfully achieved a fully in vitro generation of this ArM by PCR and cell-free extracts, establishing the foundations for a completely synthetic pathway to produce these kinds of complexes. Finally, our system also showed catalytic activity inside water-in-oil droplets, thereby paving the way for future screenings of protein libraries to improve the hemin binding pocket and thus enhance the catalytic properties of the enzyme.

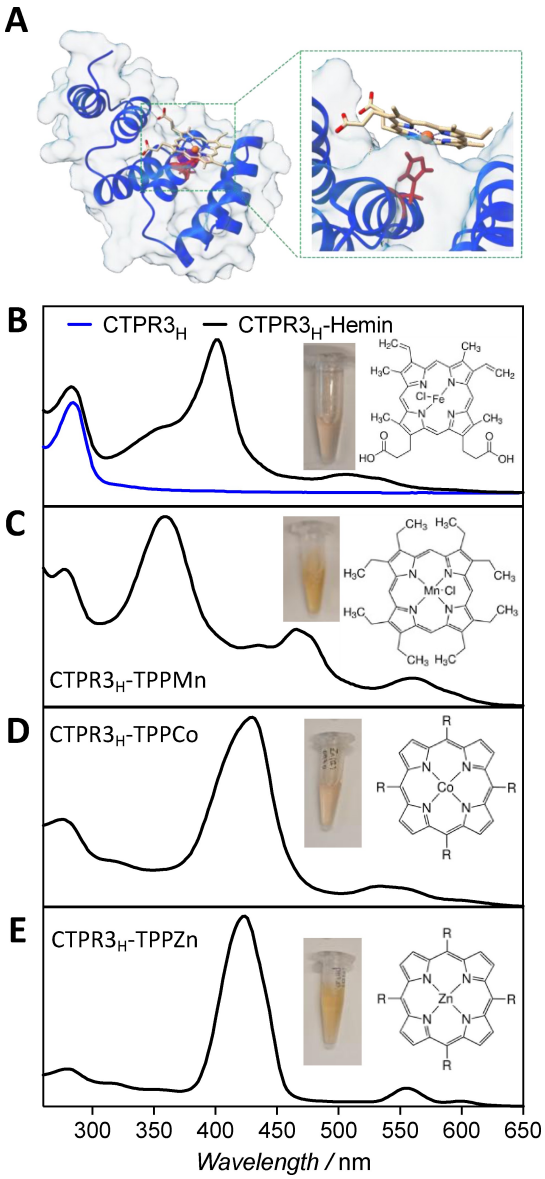

Figure 1. A) Putative structure of the CTPR3 with the N6H point mutation at the central repeat for the coordination of the hemin molecule. The molecular docking model was obtained based on the CTPR3 WT structure (PDB ID:1NA0)[27] using Rossetta Ligand software[28] (see Experimental Section). Right panel shows a zoom in of the coordination of the Fe (III) porphyrin to the histidine within the $CTPR3_H$ scaffold. B–E) UV-Vis spectra of (B) the free protein and CTPR3H-hemin, (C) CTPR3H-TPP–Mn(III), (D) CTPR3H–Co(II), and (E) CTPR3H–Zn(II) hybrids. The chemical structure of the porphyrins and pictures showing coloured solutions are depicted (R = phenyl).

Results and Discussion

Synthesis and characterization of $CTPR3_H$-Hemin biohybrids

In this work, we have selected CTPR proteins as scaffold for developing a novel artificial metalloenzyme due to their well-established robustness, stability, and suitability for biomolecular engineering.[25,26] These repeat proteins are convenient scaffolds for introducing desired mutations during the engineering process, since only a few conserved residues (8 out of 34) define

the protein fold. In this regard, the protein scaffold was constructed by three consecutive repeats of the CTPR module, being the second module engineered to include a histidine amino acid at position 6 of the repeat. This configuration rendered a protein with a molecular weight of 14.1 kDa (Figure S1), according to Matrix-Assisted Laser Desorption/Ionization Time-of-Flight (MALDI-ToF) measurement. Further, a metal-binding residue, namely, histidine, is conveniently allocated for the axial coordination of the metal centre of the metal porphyrin complex (Figure 1A). Further details on the protein design, expression, and purification are described in the *Experimental Section*.

Metal porphyrins have great potential as catalysts, yet their low solubility and tendency to form aggregates limit their use in water-based solutions. For this reason, the development of protein scaffolds such as $CTPR3_H$, with a catalytic cleft exposed to the solvent, that enables the solubilization and stabilization of the hydrophobic metal-organic molecules in an aqueous solution, is of high interest. This study attempted the coordination of assorted aromatic porphyrin derivatives to demonstrate the versatility of the $CTPR3_H$ scaffold. Among all the tested porphyrins derivatives – hemin; 5,10,15,20-Tetraphenyl-21H,23H-porphine compounds of Co, Cu, Zn, and Ni (TPP–Co, TPP–Cu, TPP–Zn, and TPP–Ni, respectively); and 2,3,7,8,12,13,17,18-Octaethyl-21H,23H-porphine manganese (III) chloride – only the iron porphyrin could be solubilized at basic pH. The preparation of the hybrids was carried out by incubating the engineered $CTPR3_H$ with the corresponding porphyrins in a 1:5 (protein:porphyrin) molar ratio in a water/DMSO mixture (details in *Experimental Section*). The generation of the hybrids using $CTPR3_H$ and the corresponding porphyrins was carried out under carefully optimized temperature and pH conditions. (Figure S2). The assembly procedure is performed at pH 10, a condition under which the protein is known to be in a partially extended conformation[24] to reduce steric impediments and foster the incorporation of the metalorganic molecule within the cleft. After the assembly, the native configuration of the protein was restored at pH 7, as evidenced by its circular dichroism spectrum (Figure S3). The $CTPR3_H$ scaffold successfully accommodated various porphyrins, including Fe, Mn, Co, and Zn variants, as confirmed by UV-Vis (Figure 1B–D and Figure S4). The resulting hybrids were stable, robust, and resistant to multiple washings and purification steps, demonstrating the versatility of the CTPR3 protein scaffold in accommodating and stabilizing porphyrin molecules. These findings have significant implications for the use of metal porphyrins as catalysts in aqueous solutions. The subsequent characterization focused on evaluating the catalytic profile of the iron-porphyrin containing hybrid, which mimics natural heme-containing enzymes such as HRP or myoglobin.

The UV-Vis spectrum of the $CTPR3_H$-hemin (Figure 1B) clearly displayed a Soret peak, a distinguishing characteristic of the Fe–N coordination present in heme proteins. Note that the hybrid showed a bathochromic shift to 409 nm compared to HRP, where the band is centred at 402 nm. Similar studies involving protein variants in which the iron porphyrin molecule is coordinated to histidine residues[29–31] have also reported a comparable shift at this wavelength. Importantly, such an absorption band was not observed when the wild-type CTPR3 protein, which lacks the coordinating His ligand, was incubated with the hemin molecule (Figure S5). Moreover, X-ray photoelectron spectroscopy (XPS) further confirmed the hemin-histidine coordination, as evidenced by the emergence of a shoulder at 398 eV in the N 1s band of the hybrid, indicating N–Fe interaction[16] (Figure S6). Therefore, the engineered histidine ligand of $CTPR3_H$ enables the precise accommodation of the hemin through a predicted axial coordination, showing an affinity binding constant (K_D) of 3.3 μM (Figure S7). Finally, while we observed that the coordination was significantly affected by acidic pH, presumably due to protonation of the histidine, we determined that the ArM was stable for over one month when stored at 4 °C (Figure S8).

Peroxidase-like activity of the ArM

Heme cofactor serves as the catalytic centre of several natural enzymes, including HRP, myoglobin and most catalases.[32] By themselves, both heme (ferrous) or hemin (ferric iron) metal-organic catalysts can perform peroxidation reactions efficiently, oxidizing a broad range of organic substrates in the presence of hydrogen peroxide. Furthermore, the catalytic activity of hemin can be enhanced when it forms complexes with other molecules such as DNA[15] or proteogenic molecules.[21] In this work, we have assessed the peroxidative capability of the novel ArM with two common substrates, i.e., 2,2'-azino-di(3-ethylbenzothiazoline-6-sulfonic acid (ABTS) and 3,3',5,5'-tetramethylbenzidine (TMB). The oxidation of ABTS and TMB in the presence of hydrogen peroxide (H_2O_2) was monitored by measuring absorbance changes at 420 and 650 nm, respectively. The hybrids exhibited Michaelis-Menten kinetics profile (Figure S9), confirming their behavior as artificial enzymes. The affinity of CTPR-hemin for TMB, with a K_M of 110.6 ± 29.1 μM, is similar to other reported hemin-loaded hybrids, which show K_M values from 0.5 to 0.1 mM.[33] Remarkably, these values are similar to that measured for natural HRP, 0.15 mM. Further, we achieved similar turnover frequencies (TOF) to those obtained by Liu et al. for hemin-loaded nanoparticles assembled by a complex combination of His-rich peptides and guanine-rich nucleotides ($TOF_{[ABTS]}$ of 0.65 *vs* 0.44 s^{-1} for CTPR-Hemin and DNA/peptide nanoparticles, respectively).[34] The measurement of the K_M with respect to H_2O_2 co-substrate provided important insights on the chemical environment in which the hemin is accommodated. We measured a K_M (H_2O_2) of 3.0 ± 0.5 mM for $CTPR3_H$-hemin (Figure S10), which is similar to other recombinant isoenzymes (3.5 mM for HRP isoenzyme recombinantly produced), yet significantly higher compared to other natural peroxidases, including natural HRP (0.06 ± 0.02 mM, as measured in this work) (Table S1). Therefore, the complex composition of the catalytic pocket in natural enzymes seems to facilitate the cleavage of the H_2O_2 for catalysis.

We also characterized the peroxidation rates of dopamine using $CTPR3_H$-Hemin. With this, we could provide valuable information to optimize the potential development of droplet-

based microfluidic screening utilizing the $CTPR3_H$ scaffold. Using a microfluidic device, fluorescent polydopamine (FPDA) production can be monitored and quantified by utilizing dopamine as a substrate. The kinetic profile of the peroxidation of dopamine was revealed by fluorescence and UV-Vis measurements, yielding similar results (Figure S11). We determined a K_M value of 43 ± 11 μM, which is significantly low compared to other natural enzymes such as catechol oxidases, and other peroxidases, with values that range in the mM.[35–37] Finally, we also observed that the ArM outperformed the uncoordinated metal-organic porphyrin in terms of TOF, with a value of 0.22 ± 0.01 s^{-1} compared to 0.099 ± 0.005 s^{-1}, respectively (Figure S12, Table S2).[38] Due to the significantly higher affinity of $CTPR3_H$-hemin towards dopamine compared to other systems (Table S1), the limited autoxidation of dopamine in the absence of the catalysts (Figure S13), and the significant difference in the catalytic rates compared to free hemin, we concluded that dopamine is a convenient substrate for the droplet-based screening developed in this work.

Catalase-like activity of the ArM

While performing the peroxidations, we detected the formation of a significant number of bubbles after the reaction, which might indicate the coexistence of a catalase-like activity in the ArM (Figure S14). This catalase-like activity is more evident at basic pH, which explains the prompt decrease of the peroxidase-like activity at pH > 7, as shown by the pH-dependent activity measured in Figure 2. The coexistence of peroxidase and catalase activity is present in several peroxidases.[39] Interestingly, these experiments showed that the optimum pH for the peroxidation reaction was significantly shifted from pH 4.0 to pH 6.0 for HRP to ArM, respectively.

The compositional and functional characterization of $CTPR3_H$-hemin has evidenced that the correct accommodation of the hemin into the protein scaffold enhances the catalytic capability of the iron porphyrin complex. The catalytic profile of the remaining porphyrin hybrids is being evaluated.

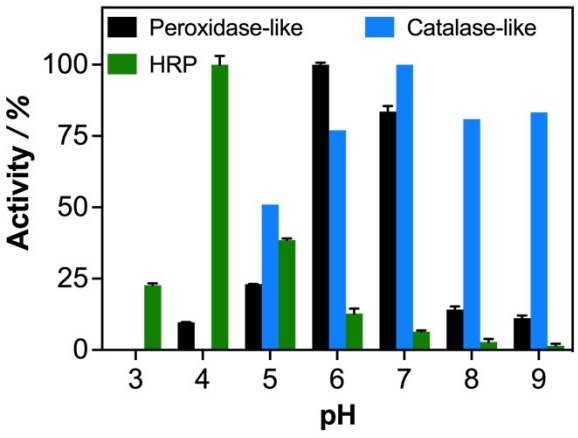

Figure 2. pH activity profile for ArM (black and blue) and HRP (green). The peroxidation activity was measured using ABTS and H_2O_2 (black and green) and the catalase-like activity was measured with H_2O_2 (blue).

A fully in vitro metalloenzyme

Given that the performance of the ArM relies on both the polypeptidic environment in which the hemin is accommodated, and the synthesis conditions used for the assembly of the hybrids, the development of synthetic methodologies to screen and optimize the fabrication of hybrid biodopamine molecules using automating processes is a central goal. For this purpose, a totally synthetic pathway to produce ArMs has been developed, aiming to avoid tedious and time-consuming steps of recombinant amplification and expression. First, the selected plasmid DNA was subjected to a circular PCR using a thermocycler (see Experimental Section).

All in vitro experiments were conducted using a plasmid where the His-Tag is off-frame to avoid interactions between the additional histidines with the hemin molecule. A cell-free in vitro transcription and translation system (IVTT) was later added to the DNA and the mixture was incubated for 2 hours. Hemin was subsequently supplemented. Finally, dopamine and H_2O_2 were added at a concentration of 1.5 mM and 50 mM, respectively. After one hour, fluorescence intensity was measured at 473 nm upon excitation from 500 to 700 nm, obtaining a peak at 525 nm, similar to the previous results obtained with the ArM fabricated by recombinant expression (Figure 3A). Once again, the comparison of the intensity between the ArM and free hemin demonstrates that engineered enzyme possesses a higher catalytic activity.

Surprisingly, the blank containing the IVTT also showed a high basal fluorescence. The kinetic behaviours of both species were also compared by measuring the fluorescence at 525 nm for 200 min. Similarly, the ArM displayed superior catalytic properties over time, reaching the maximum fluorescence after 140 min (Figure 3B). In contrast, the curve for the free hemin showed no activity and a decrease over time. This phenomenon may be attributed to hemin coordinating with surface-exposed histidine or cysteine residues present in the ribosomes or RNA polymerases within the IVTT systems, disabling them for the oxidation of dopamine. The IVTT system itself again showed a basal fluorescence but no activity.

These results show the feasibility of fabricating ArMs with peroxidase-like activity using fully synthetic pathways. However, further improvements in the performance of IVTT systems and in the fabrication workflow are still needed to achieve the yields obtained by recombinant expression systems.

Towards in emulsio enzyme improvement

The ability of this system to be fully synthetized by in vitro methods paves the way to improve its catalytic properties or discover novel ones by droplet-based screenings. To test this hypothesis, two different experiments were carried out on microfluidic chips. For this purpose, a custom inverted micro-

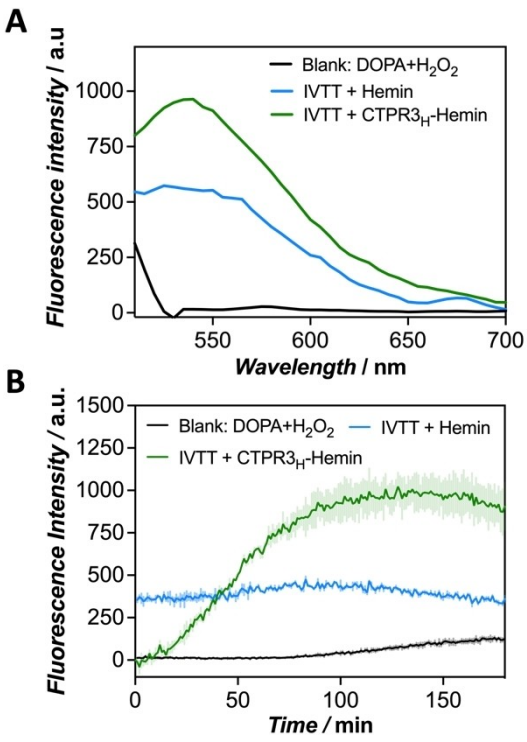

Figure 3. Fluorescence measurements performed using the IVTT system. A) Fluorescence spectra of the synthetically fabricated ArM, the hemin, the IVTT and the dopamine + H_2O_2 blank from 500 to 700 nm. The ArM, the hemin, and IVTT show a fluorescence emission peak at 525 nm when excited at 473 nm. B) Kinetic behavior of the abovementioned species. Only the ArM shows a clear catalytic activity over time.

scope with a blue laser (473 nm) focused towards the objective was built in order to measure the fluorescence of the droplets (Figure 4A), similar to other setups used elsewhere in droplet microfluidic experiments.[40,41] The first experiment consisted of encapsulating the purified ArM with H_2O_2 (25 mM) and dopamine (25 mM) within droplets. A two-inlet microfluidic chip with a nozzle of 30 μm was used to separate the catalyst from the substrate (Figure 4B). After 2 hours of incubation at 37 °C, droplets were introduced in a reservoir, and their fluorescence was examined using an epifluorescence microscope to obtain the images observed in Figure 4C for both species. The ArM and the free hemin were also excited with a 473 nm laser, and the signal was measured with a PMT (Figure 4D), resulting in an average fluorescence of 1.367 ± 0.019 a.u for the ArM. The results revealed a significant increase in the fluorescence signal at 525 nm when compared to the catalytic activity of the free hemin (Figure 4E). The representative fluorescence traces measured by the photomultiplier tube (PMT) for the ArM and the free hemin are presented in Figure 4E. Each peak represents the fluorescence of an individual drop.

In the second test, $CTPR3_H$ plasmid was encapsulated with all the necessary reagents to perform a circular droplet PCR on a drop generator chip (Figure 4F, left). The sample was later subjected to 20 cycles of amplification in the thermocycler, with ramps of 0.6 °C/min to avoid the coalescence of the drops. A portion of the emulsion was broken with perfluoroctanol, the aqueous phase was extracted, and the size of the DNA was verified on a 1 % agarose gel (Figure S15). In the next step, the remaining drops were reinjected on a picoinjection chip[42] (Figure 4F, right), and the cell-free system, dopamine (3 mM)

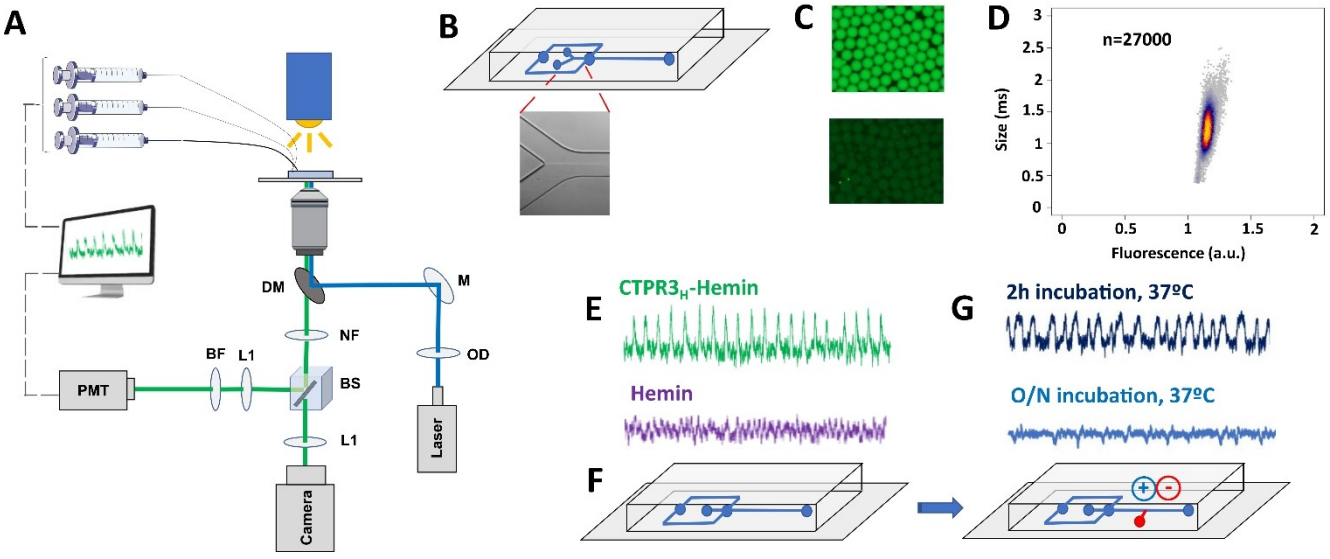

Figure 4. A) Optical setup of the microfluidic microscope. A 473 nm laser was added to an inverted microscope to measure the fluorescence of the drops (see Experimental Section). Acronyms refer to: OD: optical density filter, M: mirror, DM: dichroic mirror, NF: notch filter, BS: beam splitter, L1: low pass filter and BF: band pass filter. B) Sketch and detail of the two-inlet microfluidic chip used in these experiments. C) Epifluorescence images of the ArM (top) and hemin (bottom) catalytic activity inside the drops. D) Heatscatter graph of the catalytic activity of the ArM. The x-axis shows the fluorescence of the individual drops. The y-axis shows the size of the drops measured as the passing time through the laser. Due to the lack of peaks for the hemin signal, it was not possible to calculate the typical heat-scatter graph for these experiments. E) Sketches of the drop generator and the picoinjector used in this article. F) Fluorescence signals of the ArM and the hemin recorded by the PMT. G) Fluorescence signals of the ArM with an entirely in vitro generation after 2 and 16 hours.

and H_2O_2 (25 mM) were individually injected to all the drops following standard picoinjection conditions ($V_{peak\,to\,peak} = 200$ V, f = 20 KHz). The drops were collected in a vial and incubated at 37 °C. The fluorescence of each individual drop was measured after 2 and 16 hours (Figure 4G). The drops exhibited fluorescence after 2 hours, confirming that the *in emulsio* expression of the $CTPR3_H$, the coordination with hemin, and the catalytic reaction with dopamine took place. However, after 16 hours, the fluorescence signal of the drops diminished (Figure 4G, bottom), due to the quenching process of polydopamine, as observed in the control experiment (Figure S16). This experiment paves the way to screen different protein-based libraries to enhance the catalytic properties of ArMs since the expression and coordination of these complexes can be achieved inside drops. This high throughput *in emulsio* screenings have been widely used to improve the properties of various non-metal-based enzymes.[43–45] However, further improvement in the coordination conditions of the experiments is still needed to sort the desired variants effectively. It must be noted that to encapsulate a unique mutant per drop for further enzyme improvement experiments, the initial DNA concentration must be low enough. In droplet microfluidics, the amount of DNA molecules per drop is governed by the Poisson distribution:

$$P(X) = (\lambda X\, e\,(-\lambda))/X!$$

where P is the fraction of droplets containing X DNA molecules, and λ is the mean number of droplets. To ensure the highest number of drops with a unique DNA molecule, the value of λ should be 0.1. Thus, one should reduce the initial DNA concentration before the droplet PCR to have individual mutants within the drops.

Conclusions

In this study, we have designed an engineered CTPR3 scaffold and fabricated an ArM with remarkable peroxidase activity. Our results conclude that the $CTPR3_H$-Hemin ArM possesses better peroxidase-like activity than free hemin. The protein scaffold presumably influences the structural organization and accommodation of hemin within the protein scaffold significantly, leading to optimized interaction between the artificial catalytic center and dopamine, thereby facilitating the reaction. We have, therefore, successfully developed an ArM by mimicking the characteristics of the HRP.[46] This approach holds the potential to generate customized metalloenzymes by selectively mutating specific amino acids to coordinate, for example, porphyrins in a tailored manner, which could enhance the catalytic properties of an ArM or generate novel activities.

Moreover, we have developed an entirely synthetic pathway for fabricating these types of enzymes. The synthetic ArM also successfully catalyzed the oxidative polymerization of dopamine, obtaining a fluorescent polymer that could be tracked by fluorescence measurements. Finally, we achieved *in emulsio* coordination of the protein scaffold with hemin and verified its catalytic properties. We believe that this result could open the way for further developments of different ArMs, allowing for exploration of the fitness landscape of these compounds through screenings of different scaffold libraries.

Experimental Section

Design of the $CTPR3_H$ module. The $CTPR3_H$ module was designed by incorporating a single histidine as a metal-coordinating into the consensus tetratricopeptide repeat (CTPR) unit.[8,47] The engineered $CTPR_H$ coordinating unit contains a histidine at position 6 of the 34 amino acid CTPR sequence for hemin coordination. This unit was flanked by two wild type (WT) units, resulting in $CTPR3_H$. To enhance solubility in aqueous media, an additional C-terminal solvating helix with polar residues is included in the protein sequence.

$CTPR3_H$-hemin molecular docking. The molecular docking model shown in Figure 1A was generated using RosettaLigand software.[28] Precisely, we used Rosetta Docking&Design simulations and a customized clustering protocol to retrieve the best docking structure. Two docking constraints were introduced during the docking process: i) the distance between the N atom of the histidine and the Fe atom of the hemin should be 2.0 ± 0.5 Å,[48] and ii) the plane of the hemin molecule should be perpendicular to the histidine. The molecular model shown was the best scoring structure after the docking process.

Expression, purification, and characterization of CTPR3 proteins. The synthetic gene for the desired protein ($CTPR3_H$) was inserted in pProEx-HTA vector, coding for N-terminal hexa-histidine tag and ampicillin resistance, was expressed in *Escherichia coli* strain C41 (DE3) after induction with 1 mM isopropyl β-d-thiogalactoside (IPTG) at an optical density of 0.6–0.8 followed by 18 h growth at 20 °C. The cell pellets were suspended in lysis buffer (500 mM sodium chloride, 500 mM urea, 50 mM Tris-HCl pH 8.0) and lysed by sonication. After that, the pellet was frozen at −20 °C for at least for one day. The proteins were purified from the supernatant using standard Ni-NTA affinity purification protocol. The N-terminal hexa-histidine tag was then cleaved from the CTPR proteins using the Tobacco Etch Virus (TEV) protease. As a final step, the aqueous solutions of CTPRs were dialyzed against 10 mM phosphate buffer pH 7.4 at 4 °C using a dialysis membrane with molecular weight cut-off of 6–8 kDa. Protein concentration was estimated by UV-Visible measurements at 280 nm, using the molar extinction coefficient (ε = 43,320 $M^{-1}cm^{-1}$) calculated from the amino acid composition. To verify the purity of the protein, SDS-PAGE gels were performed (see Figure S1). In addition to this analysis, MALDI-ToF was performed for calculating the molecular weight. The MALDI/ToF-ToF MS UltrafleXtreme III mass spectrometer (Bruker) with delayed extraction (Bruker) and a pulsed N_2 laser (λ = 337 nm) controlled by Flex Control 3.3 software was used to record the Matrix Assisted Laser Desorption/Ionization time-of-flight (MALDI-ToF) spectra. For sample preparation in MALDI-ToF, the thin layer method was employed. Specifically, a drop of a saturated solution of α-Cyano-4-hydroxycinnamic acid (α-CHCA) in acetone was deposited on the MALDI target. The matrix solution was prepared by combining equal volumes (1:1 ratio, vol/vol) of a 10 mg/mL α-CHCA solution in acetonitrile (ACN) and 5% formic acid (70:30, vol/vol), along with a 10 mg/mL DHB (2,5-dihydroxybenzoic acid) solution in ACN and 0.1% TFA (trifluoroacetic acid) (70:30, vol/vol). Finally, the sample (1 μL) was mixed with the matrix solution (2 μL) and applied onto the MALDI plate, allowing it to dry naturally.

Recombinant synthesis and purification of the ArM. A solution of $CTPR3_H$ (294 μl from 34 μM stock) was prepared in a mixture of

sodium carbonate buffer (65 μL from a 500 mM stock, pH 10.0), sodium chloride (98.3 μL from a 1 M stock), and water (491 μL). Then, the specific metal porphyrin (50 μL from a 1 mM stock dissolved in DMSO) was added to the enzyme solution. The final concentration of $CTPR3_H$ in the polymerization reaction was 10 μM. The mixture (1 mL) was stirred at 1000 rpm for 16 h at 25 °C. To remove non-incorporated porphyrins, the solution was filtered using 0.22 μm PVDF filters. Finally, the pH was adjusted to pH 7 by two dialysis steps against 2 L of 30 mM Tris-HCl buffer pH 7.0 using a 10 kDa MWCO SnakeSkin membrane. The ArME concentration was determined spectrophotometrically at 280 nm ($\varepsilon_{280nm} = 4.33\times10^4\ M^{-1}cm^{-1}$). The structural integrity of the ArM was corroborated by circular dichroism.

A precise analysis of the composition of the ArM was performed by spectrophotometry and by Inductively Coupled Plasma Mass Spectrometry (ICP-MS). Thus, the protein:hemin ratio was determined spectrophotometrically, considering a ε_{412nm} of $76600\ M^{-1}cm^{-1}$ for hemin, and by ICP-MS measuring the iron content in an ArM sample at 1.2 μM. Consistent protein:hemin ratios of 1.10 and 1.26 were determined through UV-Vis and ICP-MS, respectively. We achieved ca. 100% protein recovery after the $CTPR3_H$ modification procedure. The ArMs were stored at 4°C for further characterization.

***In vitro* synthesis of the ArM**. Circular PCR was performed using complementary forward and reverse primers facing the T7 promoter area of the plasmid by standard PCR methods. The concentration of the resulting DNA product was checked by UV-Vis, and the size was determined an agarose gel. The synthesis of the ArMs was carried out using the Cell-Free S30 T7 High-Yield Protein Expression system from Promega. Samples were incubated for 2 hours following the specifications of the manufacturer. Hemin (20 μM) was subsequently added, and the samples were incubated for three additional hours. For the binding affinity (K_D) measurement, the hemin concentration was fixed to 10 μM in a Tris-HCl buffer (50 mM, pH 7.6). Hemin was titrated with increasing concentrations of $CTPR3_H$ (from 0 to 50 μM), and after 2 h of incubation at 50 °C, the UV-Vis spectra were recorded. To calculate equilibrium dissociation constants (K_D), the absorbance at 414 nm corresponding to hemin-protein coordination was plotted versus $CTPR3_H$ protein concentration. The curves were fit to a one-site binding model using the equation $Y = Ymax*[CTPR3_H]/(K_D + [CTPR3_H])$.

Catalytic characterization of the ArM and Fe (III) Hemin. The peroxidase-like activity of the ArM was tested for its ability to peroxidize dopamine in presence of hydrogen peroxide. The enzymatic-like activity of the ArM and free Hemin was evaluated following steady-state enzyme kinetics. The increase in fluorescence at 550 nm was followed over the time with Synergy H1 Hybrid Multi-Mode Microplate Reader, controlled by Gen5 Software. The measurements of the apparent Michaelis-Menten constant (K_M (mM)) of the ArM and free Hemin were carried out in 96-well plates with a total volume of 200 μL. Reaction at different dopamine concentrations (0-4 mM) were tested at a fixed concentration of hydrogen peroxide (100 mM) in 50 mM sodium phosphate at pH 7. The catalysed reaction-time curves were calculated by monitoring the fluorescence response against the oxidation of dopamine. The resulting fluorescence after the reaction was calculated by subtraction of the background from the self-oxidation of dopamine. The experiments were performed in triplicates. The extinction coefficient for dopamine used for the calculations was $3.2\times10^4\ cm^{-1}\ M^{-1}$.[49] The apparent turnover number ($^{app}k_{cat}$, (s^{-1})) of ArM was measured at a fixed concentration of hydrogen peroxide (150 mM) and dopamine (3 mM). Reactions were performed at 37 °C in a 96-well plate and at different ArM concentrations (from 0.25–2 μM).

Microfluidic device fabrication. Microfluidic chips were produced using glass substrates and poly-(dimethylsiloxane) Sylgard 184 (PDMS) with SU8-3000 negative photoresists (MicroChem Corp) moulds fabricated using standard soft lithography methods. A PDMS/curing agent mix from the Sylgard 184 kit (10% w/w) was poured on the moulds. The mixture was subsequently degassed in a vacuum chamber using a pressure pump and cured at 70 °C overnight. After extracting the PDMS from the moulds, a 0.75 mm-diameter puncher was used to drill the inlet and outlet holes. The microscope glass slides and cut PDMS pieces and were cleaned with ethanol, dried with nitrogen and exposed to an oxygen plasma treatment for 2 minutes (Plasma Chamber Diener Electronic Pico) before bonding them by manual pressure. The surfaces of the microfluidic inner channels were treated with fluorosilane (Aquapel, PPG Industries). All devices were cleansed with argon before and after Aquapel treatment.

Optical setup. The custom optical setup for fluorescence measurements was mounted on a custom Zeiss inverted microscope (Zeiss AxioVert.A1) and a breadboard from ThorLabs. Fluorescence was excited by a continuous and polarized 473 nm laser (MBL-III-473-100 mW, CNI Optoelectronics) focused directly with the objective on the drops. Filtering of the fluorescence was carried out with a band pass filter at 525 ± 50 nm width (525/50 BrightLine HC). Signal was collected by means of a photo multiplier tube (PMT) (H10723, Hamamatsu Photonics). Data was acquired with a NI field programmable gate array (FPGA) (NI USB-7845R), which was controlled by a custom LabVIEW script.

Supporting Information

The supporting information includes additional control experiments, characterization of purified $CTPR3_H$, circular dichroism, optimization of conjugation and determination of K_D, uv-vis characterization, XPS measurements, stability measurements, additional kinetic studies including K_M measurements, peroxidation of dopamine including kinetic parameters, fluorescence kinetics, catalase-like activity, and circular droplet PCR protocol.

Acknowledgements

A.M. is financed by grant 2022-FELL-000011-01 funded by Gipuzkoa Fellows Program (Diputación Foral de Gipuzkoa) and grant "EPINPOC" co-funded by AECT Euroregion New Aquitaine-Navarra-Basque Country. A.L.C. acknowledges financial support by the Agencia Estatal de Investigación, Grants: PID2019-111649RB–I00 and PID2022-137977OB-I00 funded by MCIN/AEI/ 10.13039/501100011033 and Grant PDC2021-120957-I00 funded by MCIN/AEI/ 10.13039/501100011033 and by the "European Union NextGenerationEU/PRTR". A.L.C. also acknowledges financial support from Diputación Foral de Gipuzkoa grant 2023-QUAN-000023-01. This work was performed under the Maria de Maeztu Units of Excellence Program from Q5 the Spanish State Research Agency grant no. MDM-2017-0720. A.B. gratefully acknowledges the financial support from the Spanish Research Agency (AEI) for the financial support (PID2019-110239RB–I00 and PID2022-142128NB-I00 funded by MCIN/AEI/10.13039/501100011033/ and by the "European Union NextGenerationEU/PRTR"; RYC2018-025923-I from RyC program

- MCIN/ AEI /10.13039/501100011033 and FSE "invierte en tu futuro"), BBVA Foundation - IN[21]_CBB_QUI_0086, and UPV/ EHU- GIU21-033). We thank Thomas Beneyton and J–C Baret for their relentless support with the device fabrication and the mounting of the optical setup.

Conflict of Interests

The authors declare no conflict of interest.

Data Availability Statement

The data that support the findings of this study are available from the corresponding authors upon request.

Keywords: Protein Design · Repeat Proteins · Metalloenzymes · Hemin · Microfluidics · Peroxidase · Synthetic Biology

[1] H. J. Davis, T. R. Ward, *ACS Cent. Sci.* **2019**, *5*, 1120–1136.
[2] F. Schwizer, Y. Okamoto, T. Heinisch, Y. Gu, M. M. Pellizzoni, V. Lebrun, R. Reuter, V. Köhler, J. C. Lewis, T. R. Ward, *Chem. Rev.* **2018**, *118*, 142–231.
[3] A. Angeli, F. Carta, C. T. Supuran, *Catalysts* **2020**, *10*, 1008.
[4] V. Oliveri, G. Vecchio, *Eur. J. Med. Chem.* **2011**, *46*, 961–965.
[5] S.-L. Meng, X.-B. Li, C.-H. Tung, L.-Z. Wu, *Chem* **2021**, *7*, 1431–1450.
[6] J. Z. Zhang, E. Reisner, *Nat. Chem. Rev.* **2020**, *4*, 6–21.
[7] G. L. Blatch, M. Lässle, *BioEssays* **1999**, *21*, 932–939.
[8] T. Kajander, A. L. Cortajarena, L. Regan, *Protein Design: Methods and Applications* **2006**, 151–170.
[9] E. Raven, B. Dunford, *Heme Peroxidases*, Royal Society Of Chemistry, **2015**.
[10] J. Pütter, in *Methods of Enzymatic Analysis*, Elsevier, **1974**, pp. 685–690.
[11] F. W. Krainer, A. Glieder, *Appl. Microbiol. Biotechnol.* **2015**, *99*, 1611–1625.
[12] D. P. Carvalho, C. Dupuy, *Mol. Cell. Endocrinol.* **2017**, *458*, 6–15.
[13] G. C.-H. Leung, S. S.-P. Fung, A. E. Gallio, R. Blore, D. Alibhai, E. L. Raven, A. J. Hudson, *Proc. Natl. Acad. Sci. USA* **2021**, *118*, e2104008118.
[14] J. M. Chittoor, J. E. Leach, F. F. White, *Pathogenesis-related proteins in plants* **1999**, 171–193.
[15] P. Travascio, Y. Li, D. Sen, *Chem. Biol.* **1998**, *5*, 505–517.
[16] A. Rodriguez-Abetxuko, P. Muñumer, M. Okuda, J. Calvo, M. Knez, A. Beloqui, *Adv. Funct. Mater.* **2020**, *30*, 2002990.
[17] J. Guo, Y. Liu, J. Zha, H. Han, Y. Chen, Z. Jia, *Polym. Chem.* **2021**, *12*, 858–866.
[18] A. Rodriguez-Abetxuko, A. Reifs, D. Sánchez-deAlcázar, A. Beloqui, *Angew. Chem.* **2022**, *134*, e202206926.
[19] N. Fujieda, J. Schätti, E. Stuttfeld, K. Ohkubo, T. Maier, S. Fukuzumi, T. R. Ward, *Chem. Sci.* **2015**, *6*, 4060–4065.
[20] C. T. Choma, J. D. Lear, M. J. Nelson, P. L. Dutton, D. E. Robertson, W. F. DeGrado, *J. Am. Chem. Soc.* **1994**, *116*, 856–865.
[21] F. Nastri, L. Lista, P. Ringhieri, R. Vitale, M. Faiella, C. Andreozzi, P. Travascio, O. Maglio, A. Lombardi, V. Pavone, *Chem. A Eur. J.* **2011**, *17*, 4444–4453.
[22] A. Lombardi, F. Pirro, O. Maglio, M. Chino, W. F. DeGrado, *Acc. Chem. Res.* **2019**, *52*, 1148–1159.
[23] I. Rivilla, M. Odriozola-Gimeno, A. Aires, A. Gimeno, J. Jiménez-Barbero, M. Torrent-Sucarrat, A. L. Cortajarena, F. P. Cossío, *J. Am. Chem. Soc.* **2019**, *142*, 762–776.
[24] R. López-Domene, S. Vázquez-Díaz, E. Modin, A. Beloqui, A. L. Cortajarena, *Adv. Funct. Mater.* **2023**, 2301131.
[25] A. Aires, A. Sousaraei, M. Moller, J. Cabanillas-Gonzalez, A. L. Cortajarena, *Nano Lett.* **2021**, *21*, 9347–9353.
[26] K. B. Uribe, E. Guisasola, A. Aires, E. Lopez-Martinez, G. Guedes, I. R. Sasselli, A. L. Cortajarena, *Acc. Chem. Res.* **2021**, *54*, 4166–4177.
[27] E. R. Main, Y. Xiong, M. J. Cocco, L. D'Andrea, L. Regan, *Structure* **2003**, *11*, 497–508.
[28] J. Meiler, D. Baker, *Proteins Struct. Funct. Bioinf.* **2006**, *65*, 538–548.
[29] M. K. Lykkegaard, A. Ehlerding, P. Hvelplund, U. Kadhane, M.-B. S. Kirketerp, S. B. Nielsen, S. Panja, J. A. Wyer, H. Zettergren, *J. Am. Chem. Soc.* **2008**, *130*, 11856–11857.
[30] S. Mukherjee, K. Sengupta, M. R. Das, S. S. Jana, A. Dey, *JBIC J. Biol. Inorg. Chem.* **2012**, *17*, 1009–1023.
[31] J. Kundu, U. Kar, S. Gautam, S. Karmakar, P. K. Chowdhury, *FEBS Lett.* **2015**, *589*, 3807–3815.
[32] M. Zámocký, F. Koller, *Prog. Biophys. Mol. Biol.* **1999**, *72*, 19–66.
[33] Y. Zhang, C. Xu, B. Li, *RSC Adv.* **2013**, *3*, 6044–6050.
[34] Q. Liu, H. Wang, X. Shi, Z.-G. Wang, B. Ding, *ACS Nano* **2017**, *11*, 7251–7258.
[35] E. Ghibaudi, E. Laurenti, C. Pacchiardo, G. Suriano, N. Moguilevsky, R. P. Ferrari, *J. Inorg. Biochem.* **2003**, *94*, 146–154.
[36] J. A. de Oliveira, M. P. da Silva, B. de Souza, T. P. Camargo, B. Szpoganicz, A. Neves, A. J. Bortoluzzi, *Dalton Trans.* **2016**, *45*, 15294–15297.
[37] D. Tarasek, B. Gąsowska-Bajger, B. Frąckowiak-Wojtasek, C. Kersten, M. Jewgiński, Ł. Kołodziej, R. Latajka, H. Wojtasek, *J. Mol. Struct.* **2022**, *1252*, 132169.
[38] F. Benaceur, H. Gouzi, B. Meddah, A. Neifar, A. Guergouri, *Int. J. Biol. Macromol.* **2019**, *125*, 1248–1256.
[39] J. Vlasits, C. Jakopitsch, M. Bernroitner, M. Zamocky, P. G. Furtmüller, C. Obinger, *Arch. Biochem. Biophys.* **2010**, *500*, 74–81.
[40] J. J. Agresti, E. Antipov, A. R. Abate, K. Ahn, A. C. Rowat, J.-C. Baret, M. Marquez, A. M. Klibanov, A. D. Griffiths, D. A. Weitz, *Proc. Natl. Acad. Sci. USA* **2010**, *107*, 4004–4009.
[41] L. Mazutis, J. Gilbert, W. L. Ung, D. A. Weitz, A. D. Griffiths, J. A. Heyman, *Nat. Protoc.* **2013**, *8*, 870–891.
[42] A. R. Abate, T. Hung, P. Mary, J. J. Agresti, D. A. Weitz, *Proc. Natl. Acad. Sci. USA* **2010**, *107*, 19163–19166.
[43] T. Beneyton, F. Coldren, J.-C. Baret, A. D. Griffiths, V. Taly, *Analyst* **2014**, *139*, 3314–3323.
[44] J. N. Milligan, R. Shroff, D. J. Garry, A. D. Ellington, *Biochemistry* **2018**, *57*, 4607–4619.
[45] J. M. Holstein, C. Gylstorff, F. Hollfelder, *ACS Synth. Biol.* **2021**, *10*, 252–257.
[46] B. Jiang, D. Duan, L. Gao, M. Zhou, K. Fan, Y. Tang, J. Xi, Y. Bi, Z. Tong, G. F. Gao, *Nat. Protoc.* **2018**, *13*, 1506–1520.
[47] A. Aires, I. Llarena, M. Moller, J. Castro-Smirnov, J. Cabanillas-Gonzalez, A. L. Cortajarena, *Angew. Chem. Int. Ed.* **2019**, *58*, 6214–6219.
[48] R. N. Samajdar, D. Manogaran, S. Yashonath, A. J. Bhattacharyya, *Phys. Chem. Chem. Phys.* **2018**, *20*, 10018–10029.
[49] L. Guo, Y. Zhang, Q. Li, *Anal. Sci.* **2009**, *25*, 1451–1455.

Manuscript received: October 4, 2023
Accepted manuscript online: December 25, 2023
Version of record online: December 25, 2023